



Distinguish the effect of Cu additive on complex electrical (dielectric/impedance) behaviors of ZnO thin films

M. E. Sayed · S. S. Fouad · E. Baradács ·
L. I. Soliman · N. F. Osman · M. Nabil ·
Zoltán Erdélyi

Received: 8 January 2024 / Accepted: 18 June 2024
© The Author(s), under exclusive licence to Springer Nature B.V. 2024

Abstract The copper element (Cu) substituted ZnO with the common formula $\text{ZnO}_{70}/\text{Cu}_x/\text{ZnO}_{70}$ ($x = 20, 50, \text{ and } 70 \text{ nm}$) was manufactured using ALD and Dc magnetron sputtering techniques, as a function of the concentration of Cu as interlayer. The effect of the amount of Cu doped in ZnO on the character and dielectric and impedance properties was evaluated. Scanning electron microscopy (SEM) and grazing incident X-ray diffraction (GIXRD) were used to

assess the microstructure of the prepared thin films and to obtain grain size measurements. The dielectric properties (ϵ' , ϵ'') and the real part of the complex electric modulus (M) were studied as a function of frequency and temperature. A strong dependence and correlation between the dielectric properties and the thickness of the Cu interlayer were investigated. The electrical impedance at different temperatures exhibited a single semicircle, indicating that the response arose from a single capacitive element corresponding to the grains. The conduction of grains and grain boundaries is detected from a complex impedance spectrum by fitting the Nyquist plot with an appropriate electrical circuit. It was revealed that the increase of the thickness of the Cu interlayer of the ZnO/Cu/ZnO system leads to a high dielectric constant and a low value of the real part of the complex electric modulus, which are very good candidates for microwave semiconductor devices and various microelectronic applications.

M. E. Sayed · N. F. Osman
Basic Science Department, Modern Academy
for Engineering and Technology in Maadi, Cairo, Egypt

S. S. Fouad
Department of Physics, Faculty of Education, Ain Shams
University, Cairo 11566, Egypt

E. Baradács
Department of Environmental Physics, Faculty of Science
and Technology, University of Debrecen, Poroszlay u.6,
Debrecen 4026, Hungary

E. Baradács · Z. Erdélyi
Department of Solid-State Physics, Faculty of Science
and Technology, University of Debrecen, P.O. Box 400,
Debrecen, 4002, Hungary

L. I. Soliman
Department of Solid-State Physics, Physics Research
Institute, National Research Centre, Cairo, Egypt

M. Nabil (✉)
Department of Basic Engineering Sciences, Faculty
of Engineering (Shoubra), Benha University, Benha, Egypt
e-mail: mohammed_diab35@yahoo.com

Keywords ZnO/Cu/ZnO · Dielectric constants ·
Complex real electric modulus · Impedance
spectroscopy studies · Multilayer nanostructures

Introduction

The complex electrical properties of any material define its characteristic role in nanotechnology applications. In recent years, interest in the use of

dielectric materials and their applications in electrical insulation and integrated circuits has increased. The dielectric properties (dielectric constants and dielectric loss) are a valuable source of information on the electrical properties of ions, atoms, and molecules, and, above all, their behavior in materials [1–4].

There are different nanostructures, such as metal, metal oxide, and multilayer nanostructures. Among these oxides, zinc oxide (ZnO) exhibits a high dielectric constant, thermal and chemical stability, and low electrical resistivity; therefore, ZnO can be used in an enormous area of applications [5–8].

Dielectric spectroscopy is a standard technique for the characterization of dissipation properties and energy storage. This application can be achieved by doping ZnO (with, e.g., Ag, Fe, Mn, Cu). For the realization of dielectric spectroscopy measurements (dielectric constant and loss factor), the host material must have one of the following phenomena, such as ferroelectricity, hopping charge transport, metal-insulator transition, the surface barrier layer capacitance, or interface effects [9–11].

Recently, defect engineering approaches have been used to achieve high dielectric constants in oxide-based materials [12–15]. The major concern of the current approach is to identify the relaxation processes and hopping dynamics of the multilayer ZnO/Cu/ZnO sample at different frequencies and temperatures. The complex impedance spectrum is a concept that applies right across the electromagnetic spectrum to resolve the contribution of different processes in the frequency domain, for example, electronic effects, bulk effects, and the interface, viz., grain boundaries.

In the present article, we continue to evaluate the effect of Cu interlayer thickness on ZnO/Cu/ZnO by means of morphological properties using scanning electron microscopy, grazing incident X-ray diffraction and dielectric measurements, electrical modulus analysis, impedance spectroscopy, and other related parameters as a function of temperature and frequency.

Experimental procedures

Polycrystalline samples with ZnO/Cu/ZnO sandwich structure were synthesized by DC magnetron sputtering and atomic layer deposition (ALD) [9]. The prepared samples were S1 for ZnO (70 nm)/Cu (20 nm)/

ZnO (70 nm), S2 for ZnO (70 nm)/Cu (50 nm)/ZnO (70 nm), and S3 for ZnO (70 nm)/Cu (70 nm)/ZnO (70 nm). Experimental illustration of preparation steps is as follows: (i) growth of 70 nm thick ZnO by ALD on Si substrate; (ii) growth of 20 (sample S1), 50 (sample S2), and 70 nm (sample S3) Cu by magnetron sputtering on ZnO layer; (iii) growth of 70 nm thick ZnO by ALD on Cu layer as seen in Fig. 1. The ZnO thin film was used as sandwich structure, with a top and bottom layers, and was deposited with constant thickness via atomic layer deposition (ALD), while the Cu layer was inserted between the top and bottom of ZnO layers and was deposited via Dc magnetron sputtering at 200 °C, with a base pressure of $\sim 5 \times 10^{-7}$ mbar. The film thickness of the three samples was precisely controlled through the number of ALD cycles and checked by a profilometer and a spectroscopic ellipsometer. More details concerning the deposition and the overall process of the preparation of the thin films were reported in our previous paper [10].

The structure of S1, S2, and S3 was studied by grazing incident X-ray diffraction (GIXRD, Rigaku SmartLab). Film morphology was investigated with the aid of a scanning electron microscope (SEM, Thermo Scientific Scios 2). From the AC conductivity measurements for the three samples under investigation, we were able to determine the maximum barrier height, activation energy, sheet resistance, and average hardness. In the present study, dielectric measurements including the dielectric loss factor ϵ'' , the permittivity (dielectric constant) ϵ' , the electric impedance (Z) of the samples, and the real part of the complex electric modulus (M) were carried out over the frequency range from 1 Hz to 100 kHz at different temperatures (293–423 K) using a programmable automatic LCR bridge Keysight E4991B impedance analyzer (NOVOCONTROL). The spectra of the parameters (ϵ' , ϵ'' , M , and Z) of samples S1–S3 were determined using the equations described in detail elsewhere [16].

Results and discussion

Structure

GIXRD patterns of samples S1–S3 grown on a Si(100) substrate are presented in Fig. 2. As can

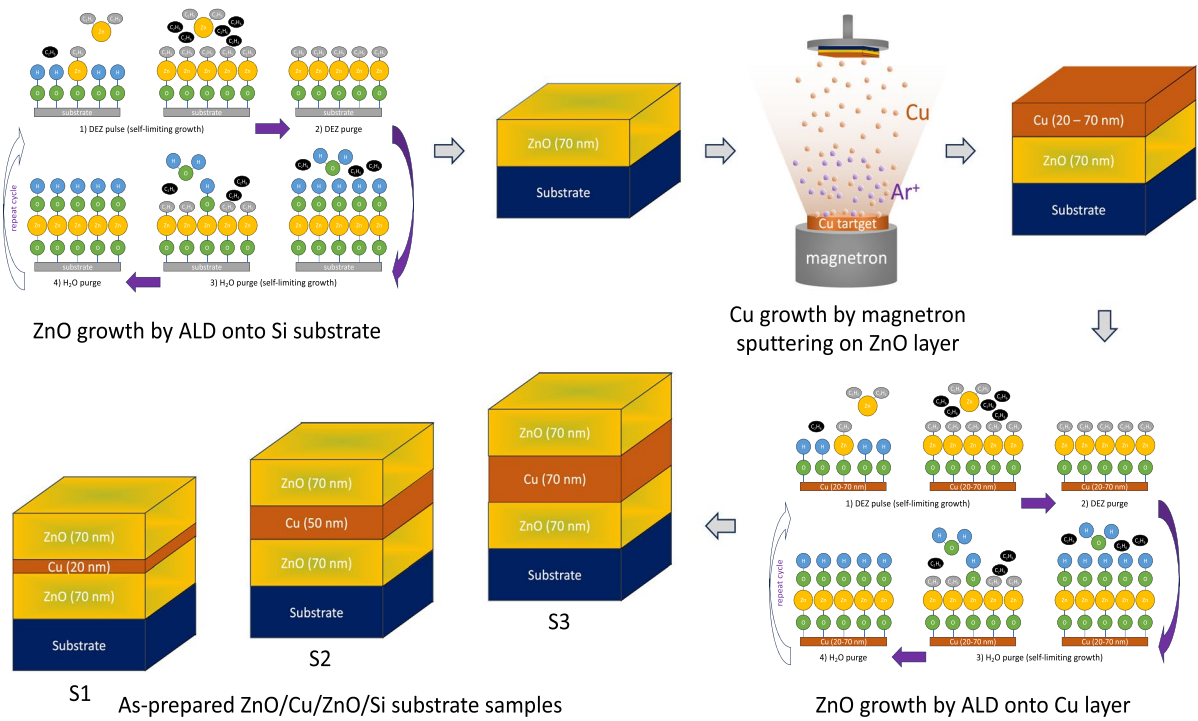


Fig. 1 Schematic drawing of S1, S2, and S3 sandwich structures

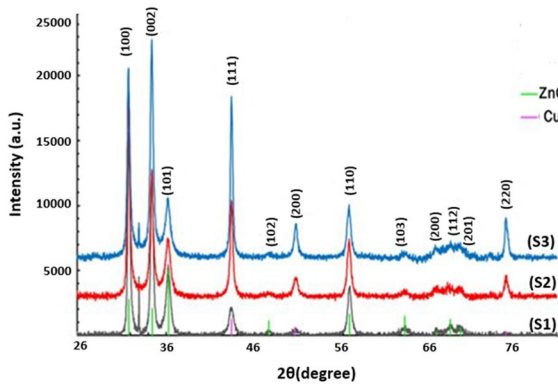


Fig. 2 GIXRD patterns of samples S1, S2, and S3

be seen for sample S1, Cu and ZnO are crystalline. Some CuO is also seen. This can be connected to the high affinity of Cu to O and considering that Cu layer is thin (20 nm only).

Figure 2 presents the GIXRD patterns of samples S1–S3. The sharp peak at 33° for samples S1 and S3 is known as the forbidden reflection of Si (substrate). Although we were able to make the main peak of Si invisible by tilting the substrate, the forbidden peak

Table 1 Roughness and crystallite size of the Cu interlayer for samples S1–S3

Samples	Crystallite size (D) (nm)	Roughness (nm)
S1	8.64	3.0 ± 0.04
S2	11.60	2.2 ± 0.09
S3	12.05	1.8 ± 0.02

can be visible at certain rotation angles [15]. The graph above shows the main benefits of ALD over its competitors, that is, chemical co-precipitation [16], co-sputtering [17], and simultaneous RF magnetron sputtering [18]. The effect of the preferential growth of Cu is indicated by the increase in the intensity of the peak belonging to Cu(111). Our results agree well with that of [19]. The crystallite sizes were determined from the GIXRD patterns and are listed in Table 1. To deduce the average value of surface roughness (±3 nm), we used spectroscopic ellipsometer and profilometer data seen in Table 1.

As can be seen, the roughness decreased from 3.0 ± 0.04 to 1.8 ± 0.02 nm with increasing thickness of

the Cu interlayer. Consequently, the surface is more uniform. The crystallite size increased from 8.64 to 12.05 nm. Figure 3 shows the surface morphology of the thin film samples under investigation. One can see a clear increase in the agglomeration of the nanoparticles accompanied by an increase in crystallite size, as seen in Table 1. Coverage with subsequent increase in Cu interlayer thickness (SEM) shows that the surface roughness is effectively reduced, with a more uniform surface. The grain growth of the crystal size due to the agglomeration, coalescence and aggregation events during the deposition process, causes the improvement, as illustrated in Table 1.

Dielectric constants (ϵ' and ϵ'')

The dielectric properties of any system define its characteristic role in electronics, which plays an important role in the performance of devices. The behavior of ϵ' and ϵ'' for S1, S2, and S3 samples as a

function of frequency in the range 0 Hz – 6×10^4 Hz at $T = 363$ K is illustrated in Fig. 4a, b.

As seen at a constant temperature, the behavior of the dielectric constants ϵ' and ϵ'' for S1–S3 samples is similar, all of them rapidly decrease at initial frequencies and slow at upper frequencies and are almost constant in the higher frequency regions. This behavior can be assigned to the fact that at low frequencies, several types of polarization contribute to the value of the dielectric constant due to the localized Guion motion within the ZnO network [17, 18], increasing the frequency with which the electric dipoles can no longer be affected by the variation of the electric field [19]. At higher frequencies, the observed dielectric constants ϵ' and ϵ'' are almost frequency-independent due to interfacial polarization [19]. It is also observed that the dielectric constants ϵ' and ϵ'' depend on the Cu concentration throughout the frequency range. The increase in the Cu interlayer content within the ZnO nanoparticles increases the permittivity

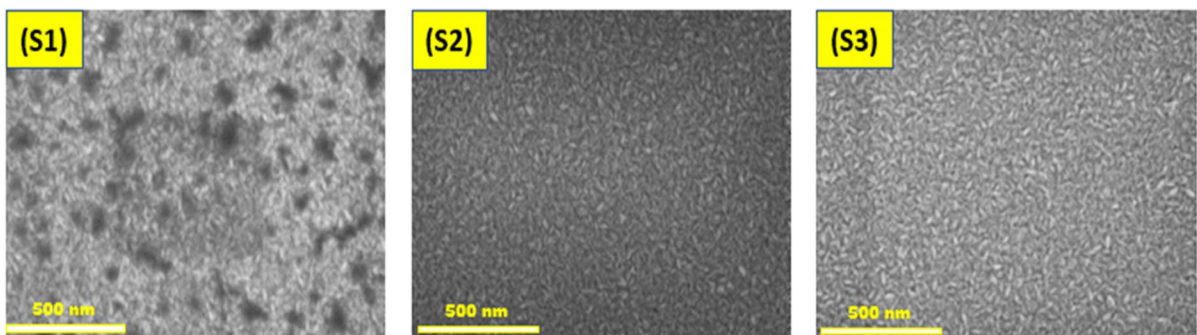
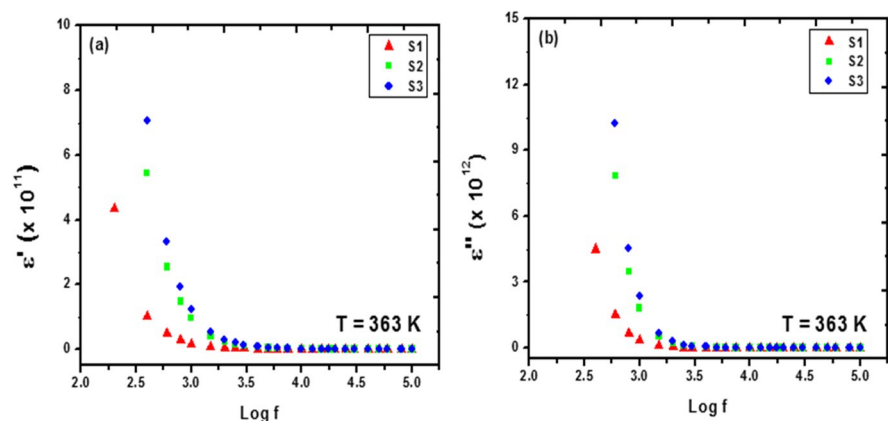


Fig. 3 SEM images for S1, S2, and S3

Fig. 4 a, b Dielectric constants (ϵ' and ϵ'') versus frequency at constant temperature for S1–S3



and improves its stability at high frequencies. The observed results are very encouraging for microwave applications [20, 21]. The ϵ' and ϵ'' of the investigated S1, S2, and S3 as a function of temperature at a constant frequency $f = 3\text{KHz}$ are shown in Fig. 5a, b.

As seen, the two graphs of ϵ' and ϵ'' have relatively similar behavior to each other, and the values of the real and imaginary parts of the dielectric constants increased with increasing Cu interlayer thickness. As we know, ZnO is one of the materials that can provide greater dielectric constants after doping it with some other metals, in our case Cu, so it can meet the need for energy storage devices. In addition to temperature and frequency dependence, the values of the dielectric constants (ϵ' and ϵ'') are also affected by the microstructural properties. Therefore, increasing the crystallite size increases the value of the dielectric constants because large particles contain a larger number of dipoles that are aligned under the influence of the electric field, leading to a larger permittivity. The variation in the crystallite sizes that had been calculated from GIXRD for samples S1–S3 that is accessible in our previous studies [9, 10] confirms the above suggestion that the crystallite size increased with increasing interlayer thickness of Cu.

Real part of the complex electric modulus (M)

The real part of the complex electric modulus (M) emphasizes the grain boundary conduction process and is suitable for determining the conductivity relaxation times (Fig. 6).

Fig. 5 a, b Dielectric constants (ϵ' and ϵ'') versus temperature for S1, S2, and S3 at constant frequency

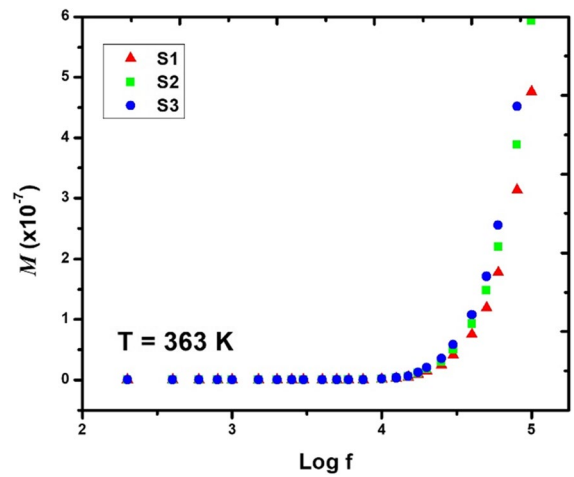
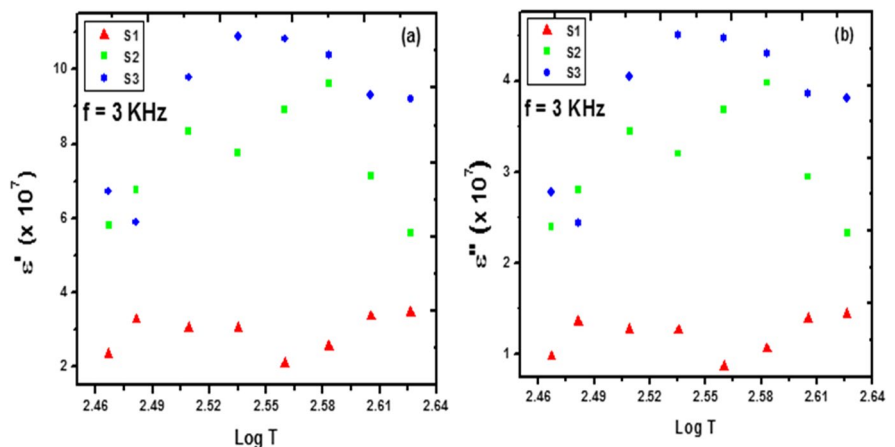


Fig. 6 Real part of the complex electric modulus (M) versus frequency at constant temperature for S1–S3

$$M = \frac{\epsilon'}{\epsilon'^2 + \epsilon''^2} \tag{1}$$

The observations show that the real part of the complex electric modulus for the three samples is close to zero in the low-frequency range. At low frequencies, M goes close to zero because the electrode effect has an influence on the total impedance. However, the magnitude of M increases with increasing frequency and reaches a constant value at a specific frequency, depending on the thickness of the Cu layer in the ZnO/Cu/ZnO system. The real part of the complex electric modulus shows that the film quality improved with increasing Cu concentration. Changes

in the lattice constants affect the bond length of ZnO by increasing the crystal size with increasing Cu interlayer thickness [22]. In our data, the low values of M in low-frequency areas indicate the transition from long range to short range hopping with increasing frequency. The increase in M with increasing frequency proves that the conduction mechanism corresponds to a transition of the short-range movement of charge carriers in the grains and grain boundaries of the ZnO/Cu/ZnO samples. From the above discussion, the shift from long range to short range is responsible for the observed movement of the charge carriers at different frequencies and temperatures.

Complex impedance analysis

The analysis of the complex impedance is one of the most effective techniques, which can be used to resolve the contributions of electrode effects and bulk effects, viz., grain boundaries, in the frequency domain and to analyze the electrical transport phenomenon and the relaxation mechanism in the material. In multilayer films with sufficiently large differences between the conductivity values of the layers, the impedance can vary considerably at relatively low frequencies. The complex impedance Z^* can be described by the following expression in the series case: ($Z^* = Z' + Z''$), where Z' and Z'' are the real and imaginary parts of the complex impedance, respectively. The complex impedance (Z^*) is related to the real (ϵ') and imaginary (ϵ'') parts of the complex dielectric constant by the following relations [23]:

$$Z' = \frac{1}{2\pi f C_o} \left[\frac{\epsilon'}{\epsilon'^2 + \epsilon\epsilon^2} \right] \quad (2)$$

$$Z'' = \frac{1}{2\pi f C_o} \left[\frac{\epsilon\epsilon''}{\epsilon'^2 + \epsilon\epsilon^2} \right] \quad (3)$$

where C_o is the capacitance of the vacuum and the angular frequency $\omega = 2\pi f$. Figure 7 shows the variation in the real and imaginary parts of the complex impedance in relation to ($\log f$) in the temperature range (293–423 K) for S1–S3, respectively.

With increasing frequency, Z' decreases, while Z'' increases for the three samples under investigation; this trend persists up to a certain frequency in which Z'' reaches a maximum value, and above “ $\log f = 4$,” both values merge on the x -axis. This tendency of

impedance with frequency provides an indication of an increase in conductivity with temperature and frequency. The fast decrease in Z' at lower frequencies is due to the significant effect of polarization (interfacial polarization and orientational polarization of dipoles) [24, 25] of the sample, while the dispersion in Z' exhibits a saturation tendency at higher frequencies, which is likely related to the rotational displacement of the dipoles. On the other hand, Z'' slowly decreases to a minimum value that corresponds to some relaxation phenomena in the sample, then increases dramatically with increasing frequency to reach a maximum value named a relaxation frequency f_r or f_{\max} , where ($f_r = 2\pi \tau$)⁻¹ and τ is called relaxation time [26]. In the higher frequency region, the imaginary part Z'' decreases rapidly and exhibits a saturation tendency. This behavior of (Z'') with a broad peak indicates a relaxation process in the films under study. Figure 8a, b shows the frequency dependence of Z' and Z'' for the three samples at constant temperature $T = 363$ K.

It appears that both Z' and Z'' decrease with increasing Cu interlayer thickness and that the values of the relaxation frequency or the maximum frequency “ f_{\max} ” indicate a monotonous decrease with increasing thickness of the Cu interlayer, which is a typical behavior of semiconductor materials. The previously provided behavior of the optical energy gap and the electronegativity for the same samples under study supports the above explanation, where they were found to decrease with increasing thickness of the Cu interlayer [9]. The shift and broadening of the peak can be explained in terms of grain boundaries [27]. Any results obtained for the difference in electronegativity between layers are expected to play a fundamental role in the variation of optical properties and complex impedance as well [9]. The variation of f_r and τ compared to the direct optical energy gap and E_g and the average optical electronegativity $\Delta\chi$ are shown in Table 2.

Nyquist plot analysis

To evaluate complex impedance measurements, we used the Nyquist plot, also called the Cole–Cole plot [15], which is a fundamental tool in the investigation of the stability of control systems. The Nyquist plot can provide several information on the difference in the number of zeros of the transfer function for each angle at which the curve

Fig. 7 (a,a1)(b,b1) and (c,c1) Representation of Z' and Z'' versus ($\log f$) at different temperatures for S1–S3

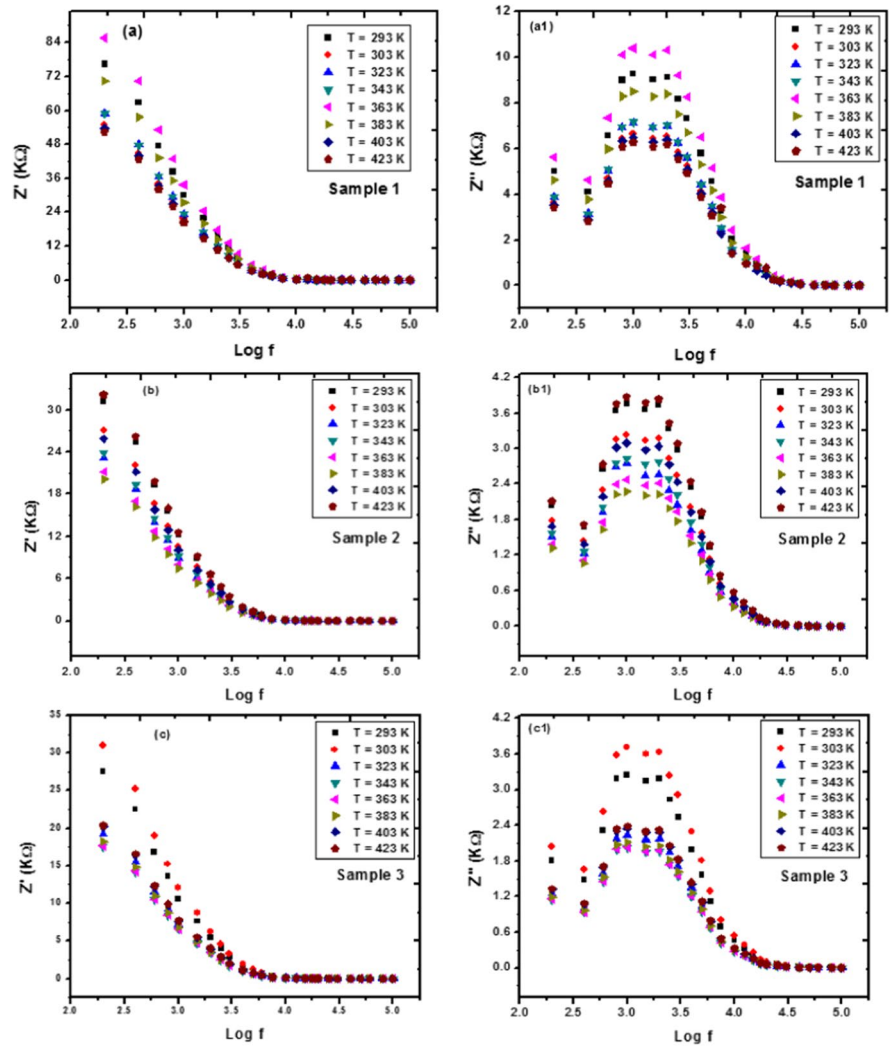
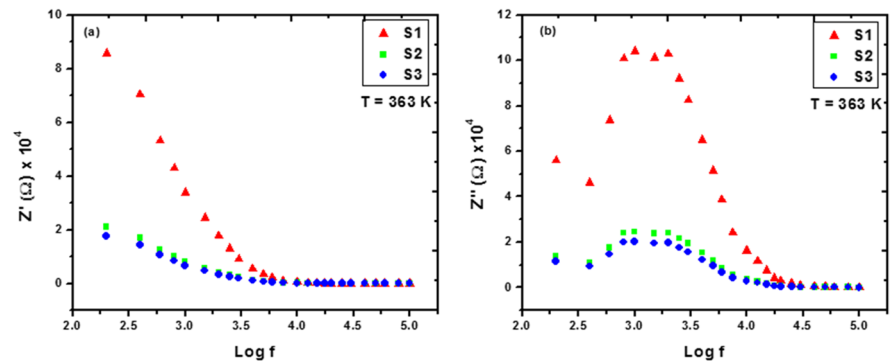


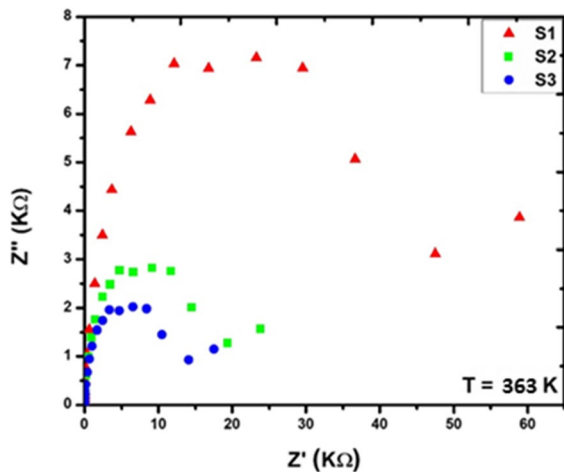
Fig. 8 a, b The variation of Z' and Z'' versus frequency at temperature 363 K for S1–S3



approaches the origin. The Nyquist plot is presented by the frequency dependence of Z' and Z'' at 363 K. Figure 9 shows the Nyquist plots of the impedances

Table 2 Values of relaxation frequency (f_r), relaxation time (τ), band gap (E_g), and electronegativity ($\Delta\chi$) for S1, S2, and S3

Sample	f_r (KHz)	τ (μ s)	E_g (eV) Ref [10]	$\Delta\chi$ Ref [10]
S1	1.288	123	2.75	0.739
S2	1.23	129	2.63	0.706
S3	1.202	132	2.43	0.653

**Fig. 9** Nyquist plot between Z' and Z'' for S1, S2, and S3 at temperature $T = 363$ K**Table 3** The resistance (R), AC conductivity (σ_{ac}), and microhardness used for samples S1–S3

Sample	R (K Ω)	σ_{ac} ($\Omega\cdot\text{cm}$) ⁻¹	Microhardness Ref [9]
S1	60	3.63×10^{-08}	643.6
S2	24	1.04×10^{-07}	556
S3	17	1.33×10^{-07}	524.3

at constant temperature ($T = 363$ K) for the three samples under investigation.

As seen, the frequency increases from the low frequency (f) on the right to the high frequency on the left; also, the semicircle starts from low and decreases in diameter and becomes more skewed as the thickness of the Cu interlayer increases [28, 29], indicating the influence of the thickness of Cu on the relaxation mechanisms. Calculated values of the resistance (R) and AC conductivity, microhardness,

and grain size of the investigated samples are listed in Table 3.

It is evident from Table 3 that R decreases with increasing thickness of the Cu interlayer. Our previous results for the same three samples of thin films of ZnO/Cu/ZnO given in [9] also confirm the decrease in R with the decrease in Vickers microhardness and the increase in grain size of S1–S3. Comparing the parameters determined with those previously determined, recorded in Tables 1, 2, and 3, we can conclude that with increasing Cu content in the ZnO/Cu/ZnO system, the average crystallite size of the prepared samples increased, the relaxation time was found to be inversely proportional to the resistance, and the conductivity was inversely proportional to the optical energy band gap. The observed improvement of the significant relations by Cu dopants can be used as excellent performance for photodiodes or detectors.

Conclusion

We reported a thorough study of how the thickness of the Cu interlayer affects the surface morphology and dielectric constants, the complex real electrical modulus, and the electrical impedance of three polycrystalline sandwich-structure-type samples of ZnO/Cu/ZnO with constant thickness of ZnO (70 nm) and variable thickness of Cu (20, 50, 70 nm). Multilayer thin film samples were synthesized by magnetron sputtering and atomic layer deposition. The GIXRD and SEM measurements confirmed that the crystallization of three sample specimens improved as the thickness of the Cu layer increased. Analysis of the dielectric constants (ϵ' and ϵ'') tendencies shows a decrease with increasing frequency and an increase with increasing thickness of the Cu interlayer thickness. The complex real electrical modulus (M) shows a gradual increase with frequency and a reduction in M with the increase in Cu. These results show an enhancement of the quality of the samples with increasing thickness of the Cu interlayer. The complex impedance spectra show the contribution of grain and grain boundary effects to electrical properties, which is endorsed by the Nyquist plots. A correlation has been observed and explained between the calculation results and the previously relevant experimental results for the “optical energy gap, electronegativity, grain size, and

microhardness” for the same samples under investigation. These comprehensive results show that the combination of ZnO/Cu/ZnO thin film systems provides optimum results in all electrical and optical properties, which can be used as a high performance in several applications.

Acknowledgements The thin film samples used in this study were prepared and characterized at the Faculty of Science and Technology, University of Debrecen, according to the agreement between the Faculty of Education, Ain Shams University “Coordinator and Supervisor Prof. Dr. Suzan Fouad,” and Faculty of Science and Technology, University of Debrecen “Coordinator and Supervisor Prof. Dr. Zoltán Erdélyi.” The dielectric and the electrical impedance were measured in the Electric and Dielectric Measurements Unit, Semiconductor Physics Laboratory (SPL) at the National Research Center (NRC) in Egypt. Project No.TKP2021-NKTA-34 has been implemented with the support provided from the National Research, Development and Innovation Fund of Hungary, financed under the TKP2021-NKTA funding scheme.

Author contribution S.S. Fouad: the idea and the writing and the revision; Eszter Baradács: prepared samples and made the characterizations; N.F. Osman and M.E. Sayed: calculated the different parameters and prepared the results; L. I. Soliman: following up all the measurements and revision; M. Nabil: calculated the different parameters and prepared all the figures in the final form and responsible on the correspondence; and Zoltán Erdélyi: preparation, ellipsometry measurements, and supervising all the characteristics that had been made in Debrecen, revision

Data availability All data generated or analyzed during this study are included in this published article.

Compliance with ethical standards

Ethical approval Not Applicable.

Conflict of interest The authors declare that they have no conflict of interest.

References

- Tariq H, Azad F (2022) Functional properties of donor (Al) and acceptor (Cu) cooped high dielectric constant ZnO nanoparticles. *J Nanomater* 2022(1):3855582
- Younas M, Zou LL, Nadeem MSSC et al (2014) Impedance analysis of secondary phases in a Co-implanted ZnO single crystal. *Phys Chem Chem Phys* 16(30):16030–16038
- Fouad SS, Sakr GB, Yahia IS, Basset DMA (2011) Structural characterization and novel properties of defect chalcopyrite ZnGa₂Te₄ thin films. *Mater Res Bull* 46(11):2141–2146
- Zaka H, Parditka B, Erdélyi Z, Atyia HE, Sharma P, Fouad SS (2020) Investigation of dispersion parameters ,dielectric properties and opto-electrical parameters of ZnO thin film grown by ALD. *Optik* 203:163933
- Abdel-Basset DM, Mulmi S, El-Bana MS, Fouad SS, Thangadurai V (2017) Structure ,ionic conductivity ,and dielectric properties of Li-rich garnet-type Li_{5+2x}La₃Ta_{2-x}Sm_xO₁₂(0≤x≤0.55) and their chemical stability. *Inorg Chem* 56(15):8865–8877
- Fouad SS, Atyia HE (2016) Investigation of ac conductivity ,dielectric and thermodynamics properties of SeTePb glassy system. *J Alloys Compd* 28(11):1206–1213
- Pal SK, Mehta N, Fouad SS, Atyia HE (2020) Dielectric behavior of amorphous thin films of Se-Te-Sn-Ge. *Solid State Sci* 104:106289
- Hu W, Liu Y, Withers RL et al (2013) Electron-pinned defect- dipoles for high-performance colossal permittivity materials. *Nat Mater* 12(9):821–826
- Fouad SS, Soliman LI, Baradács E, Sayed ME, Parditka B, Osman NF, Nabil M, Erdélyi Z (2023) Advances for enhancing the electrical properties and microhardness activity of ZnO/Cu/ZnO thin films prepared by ALD. *J Mater Sci* 58(15):6632–6642
- Fouad SS, Parditka B, Nabil M, Baradács E, Negm S, Erdélyi Z (2022) Effect of Cu interlayer on opto-electrical parameters of ZnO thin films. *J Mater Sci: Mater Electron* 33:20594–20603
- Fouad SS, Parditka B, Atyia HE, Baradács E, Bekheet AE, Erdélyi Z (2022) AC conductivity and dielectric parameters studies in multilayer TiO₂/ZnO thin films produced via ALD technique. *Chin J Phys* 77:73–80
- Fouad SS, Parditka B, Atyia HE, Baradács E, Erdélyi Z (2022) The real role of Cu metallic interlayer on the dielectric dispersion and conduction mechanism of TiO₂/Cu/TiO₂ nanolaminates. *Optics* 260:169078
- Mehta N, Fouad SS, Baradács E, Parditka B, Pal SK, Erdélyi Z (2023) Multilayer stack structural designing of titania and zinc white using atomic layer deposition (ALD) technique and study of thermally governed dielectric dispersion and conduction under alternating electric fields. *J Mater Sci: Mater Electron* 34(8):708
- Mohammed MI, Fouad SS, Mehta N (2018) Dielectric relaxation and thermally activated AC conduction in (PVDF)/(rGO) nano-composite role of rGO over different fillers. *J Mater Sci: Mater Electro* 29:18271–18281
- Graca M, Valente MA, Ferreira da Silva MG (2003) *J Non-Cryst Solids* 325(1-3):267–274
- Rabizadeh M, Ehsani MH (2022) Effect of heat treatment on optical, electrical and thermal properties of ZnO/Cu/ZnO thin films for energy-saving application. *Ceram Int* 48(11):16108–16113
- Bergo P, Pontuschka WM, Prison JM (2007) *Solid State Commun* 141(10):545–547
- S. Sagadevan, K. Pal, Z. Z. Chowdhury, M. E. Hoque (2017) *J Sol-Gel Sci Technol* 1
- Assar ST, El-Ghazzawy EH, Abosheishasha HF (2022) Study on dielectric properties, electric modulus, and impedance spectroscopy of Ni–Ca ferrite nanoparticles. *Mater Chem Phys* 287(1):126336

20. Salman F, Khalil R, Hazaa H (2014) Dielectric studies and Cole-Cole plot analysis of silver- ion conducting glasses. *Access Int J* 3(1)
21. Selmi A, Fkiri A, Bouslimi J, Besbes H (2020) Improvement of dielectric properties of ZnO nanoparticles by Cu doping for tunable microwave devices. *J. Mater Sci: Mater Electron* 31:18664–18672
22. Belkhaoui C, Lefi R, Azabi N, Smaoui H (2018) Synthesis and electrical properties of Mn doped ZnO nanoparticles. *J Mater Sci, Mater Electron* 29:7020–7031
23. Choudhary R, Pradhan DR, Tirado C, Bonilla G, Katiyar R (2007) Effect of La substitution on structural and electrical properties of Ba(Fe₃W₁/30O₃) nanoceramics. *J Mater Sci* 42:7423–7432
24. Soltan WB, Nasri S, Lassoued MS, Ammar S (2017) Structural, optical properties ,impedance spectroscopy studies and electrical conductivity of SnO₂ nanoparticles prepared by polyopl method. *J Mater Sci: Mater Electron* 28:06649–06656
25. Coşkun M, Polat Ö, Coşkun FM, Durmuş Z, Çağlar M, Türüt A (2018) The electrical modulus and other dielectric properties by the impedance spectroscopy of LaCrO₃ and LaCr_{0.90}Ir_{0.10}O₃ perovskites. *RSC Advances* 8(9):4634–4648
26. Hayat K, Nadeem M, Iqbal MJ, Rafiq MA, Hasan MM (2014) Analysis of electro-active regions and conductivity of BaMnO₃ ceramic by impedance spectroscopy. *Appl Phys A Mater Sci & Proc* 115:1281–1289
27. Miah MJ, Akther Hossain AKM (2016) *Acta Metal Sin (Engl Lett)* 29(6):505–517
28. Rhouma FIH, Dhahri A, Dhahri J, Valente MA (2012) Dielectric, modulus and impedance analysis of lead-free ceramics. *Appl Phys A* 108:593–600
29. Pratap A, Joshi NJ, Rakshit PB, Grewal GS, Shrinet V (2013) International Journal of Modern 38 Physics: Conference Series. *World Sci Publishing Company* 22:1–10

Publisher's note Springer Nature remains neutral with regard to jurisdictional claims in published maps and institutional affiliations.

Springer Nature or its licensor (e.g. a society or other partner) holds exclusive rights to this article under a publishing agreement with the author(s) or other rightsholder(s); author self-archiving of the accepted manuscript version of this article is solely governed by the terms of such publishing agreement and applicable law.